ACS OMEGA

Open Access

http://pubs.acs.org/journal/acsodf

Article

Enhanced Visible-Light Photodetection with Undoped and Doped ZnO Thin-Film Self-Powered Photodetectors

Manohar Singh, Anit Kumar Ambedkar, Shrestha Tyagi, Ashwani Kumar,* Arun Kumar, Yogendra K. Gautam, Kavita Sharma, and Beer Pal Singh*

Cite This: *ACS Omega* 2023, 8, 36966−36977

Read Online

ACCESS | Metrics & More | Article Recommendations

ABSTRACT: Photodetection plays an essential role in the visible-light zone and is important in modern science and technology owing to its potential applications in various fields. Fabrication of a stable photodetector remains a challenge for researchers. We demonstrated a high-response/recovery and self-powered undoped ZnO (UZO) and Cu-doped ZnO (CZO) thin film-based visible-light photodetector fabricated on a cost-effective Si substrate using reactive cosputtering. The structural, morphological, and optical properties of CZO and UZO thin films have been examined using X-ray diffraction, field emission scanning electron microscopy, X-ray photoelectron spectroscopy, atomic force microscopy, and photoluminescence spectroscopy. The results of the CZO/n-Si photodetector compared with those of the undoped ZnO (UZO)/n-Si photodetector show that the CZO/n-Si exhibits a higher on/off ratio, responsivity, and detectivity than UZO/n-Si. Also, the CZO/n-Si photodetector shows high stability and reproducibility over 20 cycles after 180 days. A relative study of CZO/n-Si- and UZO/n-Si-based photodetectors reveals the enhanced performance of the CZO/n-Si photodetector, which has a high on/off ratio of ∼300 with a high specific detectivity of 2.8×10^{10} Jones for 75 mW visible light. The prepared self-powered CZO/n-Si/Ag thin film-based visible-light photodetector paves the way for the development of high-performance photodetector designs.

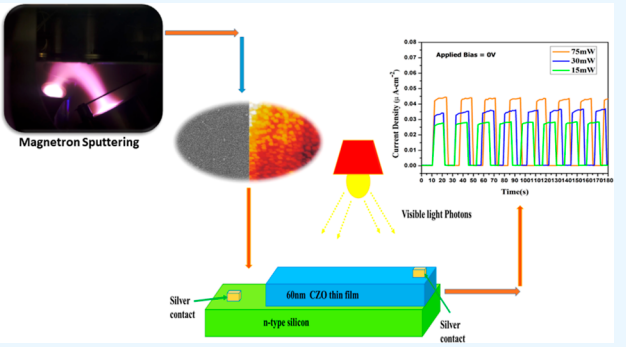

1. INTRODUCTION

In the past couple of years, the scientific community has been actively developing energy-efficient and sustainable energy detection systems in response to the rapid increase in the population and energy consumption. Photodetectors (PDs) have gained considerable attention due to their potential applications in various fields such as military defense, space science, environmental monitoring, flame detection, optical imaging, and industrial production.[1−5] Therefore, the research and development of modern and efficient PDs have become essential in recent times.

The photoconductivity effect is the basic principle of PDs, in which when radiation falls on a wide-band-gap semiconductor, the absorption of radiation occurs, and if the energy of radiation is greater than or equal to the band gap (E_g), a pair of electron−holes (e^-−h^+) is generated. Photogenerated electrons and holes can be separated for photocurrent generation by applying an external bias voltage (conventional) or generating an internal built-in electric field (self-powered). Conventional photodetectors require an external power supply to provide the potential difference, due to which the size of the overall circuit becomes large. On the other hand, self-powered PDs do not need any external power supply because these are run by the built-in potential difference, reducing the overall circuit's size. This also has some special advantages over conventional PDs such as saving energy and being suitable for use in extreme conditions.[6,7]

The past published reports on PDs indicate that in most of the PDs, GaN and silicon have been used as absorbing layers.[8−10] However, due to the blurring of optical signals between neighboring pixels, cross-talk of optical signals, low band gap, poor efficiency, and high cost of these materials, researchers take interest in other semiconductors like ZnS, CdS, V_2O_5, CeO_2, CuO, ZnO, etc.[3,11−13] Out of these semiconducting materials, ZnO is the most preferable material for making PDs because of its unique properties like wide direct band gap (∼3.37 eV), large exciton energy (60 meV), nontoxicity, transparency, and thermal stability.[14−20] The most interesting property is its large excitonic binding energy of 60

Received: June 9, 2023
Accepted: September 14, 2023
Published: September 27, 2023

meV at room temperature, which makes ZnO an efficient light emitter.[21−24] Also, the crystal growth of ZnO is easier than that in most semiconductors. Due to these unique desirable properties, ZnO can be essentially used as a high-response photodetector (PD) which could be fabricated with both Schottky and ohmic contacts.[25] However, a key issue with pristine ZnO (also with most wide-band-gap metal oxides) is that it can work for ultraviolet (UV) photodetection, as allowed by its wide-band-gap structure,[26] while many areas require a photosensor which can detect visible light. Several past research works stated that doping of various transition metals in ZnO can tune its optical and optoelectronic properties.[27,28] The doping of cations like Al^{3+}, Cu^{2+}, Cu^{+}, Ga^{3+}, In^{+}, Ag^{+}, Mg^{2+}, Mn^{2+}, Ni^{2+}, Co^{2+}, Eu^{3+}, and Tb^{3+} effectively modify the electro-optical, morphological, magnetic, and chemical properties of ZnO-based thin films.[29−32] Due to its advantageous characteristics, including low cost, natural abundance, high conductivity, and outstanding luminescence activation in II−VI compounds, copper is an efficient dopant which creates the p-type ZnO semiconductor.[33−37] Also, the doping of copper forms deep acceptor states (electron traps) within the ZnO, which increases the electrical resistivity of the ZnO thin films.[38] The increase in resistivity reduces the background carrier concentration, lowers the dark current, and hence improves the photosensitivity of ZnO-based photodetectors ($\eta = I_{photo} - I_{dark}/I_{dark}$).[39,40]

Nowadays, various physical, as well as chemical, techniques have been used to synthesize copper-doped ZnO (CZO) thin films such as pulsed laser deposition (PLD), RF/DC sputtering, and the vapor−liquid−solid (VLS) method.[41−44] Out of these techniques, sputtering is inexpensive and one of the best techniques to synthesize uniform and adhesive films of CZO.

In this study, we aim to explore the white light photosensitivity of the CZO/n-Si heterojunction with silver (Ag) electrodes. Additionally, we investigate the structural, optical, and electrical properties of undoped ZnO (UZO) and copper-doped ZnO (CZO) thin films. These thin films are deposited through reactive cosputtering of Zn and Cu targets on an n-Si substrate, all performed at room temperature. The CZO/n-Si photodetector holds promise as a cost-effective solution and finds diverse applications, including optical imaging, industrial production, military defense, space science, environmental monitoring, and flame monitoring.

2. EXPERIMENTAL DETAILS

2.1. Materials Used. To synthesize undoped (UZO) and copper-doped (CZO) ZnO thin films, reactive cosputtering of zinc (Zn) and copper (Cu) has been done with argon (Ar) as the sputtering gas and oxygen (O_2) as the reactive gas. The zinc and copper targets with a purity of 99.99%, a diameter of 50.8 mm, and a thickness of 5 mm were used as zinc and copper sources, which were bought from S.K Novel Materials in India. The ⟨100⟩ oriented n-type silicon wafer of resistivity 10 Ω cm and substrate were used for the deposition of UZO and CZO thin films. The whole experiment was performed with Advanced Process Technology (APT), a magnetron sputtering system in Pune, India.

2.2. Synthesis and Characterization of Undoped ZnO and CZO. UZO and CZO thin films were deposited on n-silicon substrates at room temperature. Prior to starting the deposition, the substrates (n-Si) were sonicated with acetone for 30 min in a sonicator (LMUC-3) and then washed with distilled water for another 10 min. Using a turbomolecular pump supported by a rotary pump, a base pressure of 5×10^{-6} mbar was attained while maintaining a fixed 8 cm between the target and the substrate. Argon (Ar) and oxygen (O_2) were injected into the sputtering chamber through the mass flow controller with a flow rate of 20 and 5 sccm. The deposition was done at 1.0×10^{-2} mbar chamber pressure and kept constant throughout. The doping of copper was done by reactive cosputtering of copper and zinc. The zinc target was kept at DC power, and an RF power source was used to sputter the copper target. Table 1 lists the optimized sputtering process parameters, and Figure 1 shows a schematic representation of the reactive cosputtering of Cu and Zn.

Table 1. Sputtering Process Parameters for UZO and CZO Thin Films

sputtering parameters	
target	Zn/Cu
base pressure	1×10^{-6} mbar
working pressure	1×10^{-2} mbar
deposition time	10 min
deposition temperature	room temperature
target-to-substrate distance	6 cm
sputtering power	
(1) Zn (D.C)	50 W (315 V × 0.16 A)
(2) Cu (R.F)	5 W
gas flow rate	
(1) argon	20 sccm
(2) oxygen	5 sccm

The structural characteristics of undoped (UZO) and copper-doped zinc oxide (CZO) thin films were investigated using an X-ray diffractometer with Cu K_α (40 kV, 40 mA) radiation (λ_{Cu} = 1.5406 Å). Surface morphology and elemental composition were examined using a Carl Zeiss-Ultra Plus field emission scanning electron microscope. The quantitative elemental composition of UZO and CZO thin films was probed by X-ray photoelectron spectroscopy (XPS) and energy-dispersive X-ray spectroscopy (EDX). The surface topography of thin films was analyzed by atomic force microscopy (AFM) (A-100, APE Research) in noncontact mode. Photoluminescence (PL) spectroscopy (Edinburgh Instruments: FLS-980) was used in the range of 340−600 nm wavelength under an excitation wavelength of 325 nm (with a He−Cd Kimmon laser as the source) to examine the optical properties as well as radiative defect states in the thin films. Keithley-2450 was used to examine the current−voltage (I−V) and current−time (I−t) measurement of the photodetector.

2.3. Fabrication of a Photodetector Based on CZO/n-Si and UZO/n-Si Junctions. For the creation of photodetectors based on CZO/n-Si and UZO/n-Si junctions, the initial step involved the deposition of CZO and UZO thin films onto an n-Si substrate, as elaborated in Section 2.2. Subsequently, silver (Ag) contacts were established on both sides of the device (depicted in Figure 7c). These contacts possessed a surface area of 42 mm^2. In order to enhance the ohmic properties of the contacts between the electrodes and the CZO and UZO thin films, both the CZO/n-Si and UZO/n-Si junctions underwent a heat treatment at 200 °C for a duration of 10 min. These improved ohmic contacts were connected by using two pointed probes, which were then

https://doi.org/10.1021/acsomega.3c04091
ACS Omega 2023, 8, 36966−36977

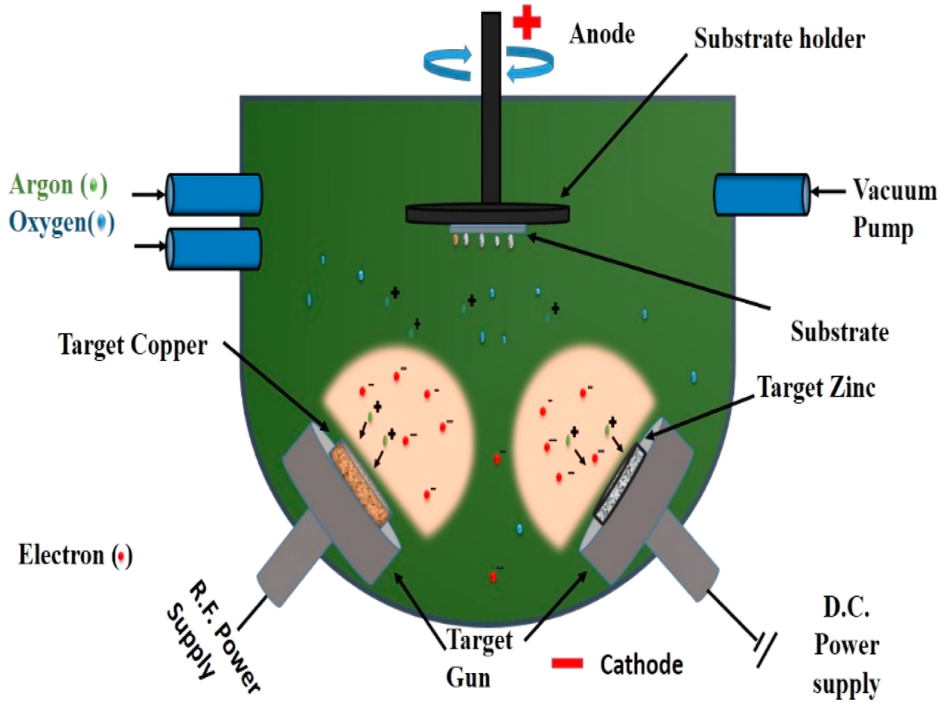

Figure 1. Schematic of the reactive co-sputtering deposition process.

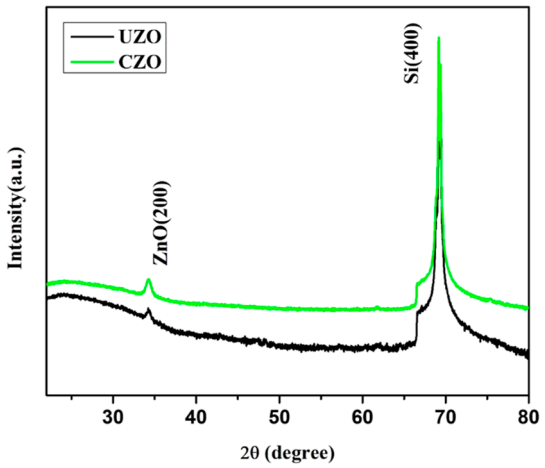

Figure 2. X-ray diffraction patterns of UZO and CZO thin films.

linked to a Keithley-2450 instrument. A visible light source, a 500 W halogen lamp, was employed, and its light intensity could be adjusted via a variable horizontal scale.

3. RESULTS AND DISCUSSION

Figure 2, illustrates the X-ray diffraction profiles of UZO and CZO thin films on n-Si(100). The XRD result reveals a hexagonal wurtzite structure for all samples with the preferred (002) plane. It implies that the *c*-axis of the crystal grains gets perpendicular to the substrate surface. This indicated that plane (002) has the lowest surface energy in ZnO crystals. As the film thickens, grains with lower surface energy become enlarged. The growth orientation then transforms into one of the lowest-surface energy crystallographic directions. As a result, the *c*-orientation may arise quickly. Undoped ZnO thin films have (002) peaks that are substantially lower in intensity than thin films with Cu doping. There are no new phases seen in the Cu-doped sample. This proves that the impurity does not alter the wurtzite structure of ZnO crystals, and it may be explained by the substitution of Cu ions for interstitial ones in the Zn lattice site. As Figure 2 shows, there is a very small shift in the peak position of (002) with Cu doping, which indicates that the Cu^{2+} ions have substituted Zn^{2+} sites without affecting the crystal structure of ZnO much. The Scherrer formula was employed to calculate the crystallite sizes of the film samples[45]

$$D = \frac{0.9\lambda}{\beta \cos\theta} \tag{1}$$

Here, λ is the X-ray wavelength (1.5406 Å), β is the full width at half maxima (fwhm), and θ is the Bragg diffraction angle.

The diffraction angle and fwhm for UZO and CZO thin films have been found to be 34.64 and 0.52 and 34.48 and 0.39°, respectively. The crystallite sizes calculated by the Scherrer formula for UZO and CZO thin films are 16.72 and 22.29 nm. Thus, crystallite size increases as we doped Cu in ZnO. This change in the crystallite size of ZnO thin films is due to the defect incorporation in the lattice site upon Cu doping.

The dislocation density serves as an indicator of the defects present in the films. For the CZO and UZO films, the respective dislocation densities (δ) were determined to be 3.57 × 10^{15} line/m^2 and 5.23 × 10^{15} line/m^2. These values are derived from the crystallite size using the Williamson–Smallman relation, as outlined in eq 2[46]

$$\delta = \frac{1}{D^2} \tag{2}$$

when two materials come into contact or are stacked together and possess distinct crystal lattice properties, such as varying lattice constants or unit cell diameters, this is termed a lattice mismatch. Such a mismatch can induce strain within the crystal structures of the materials, leading to what is known as microstrain. The microstrain within the UZO and CZO films was quantified using eq 3[46]

https://doi.org/10.1021/acsomega.3c04091
ACS Omega 2023, 8, 36966−36977

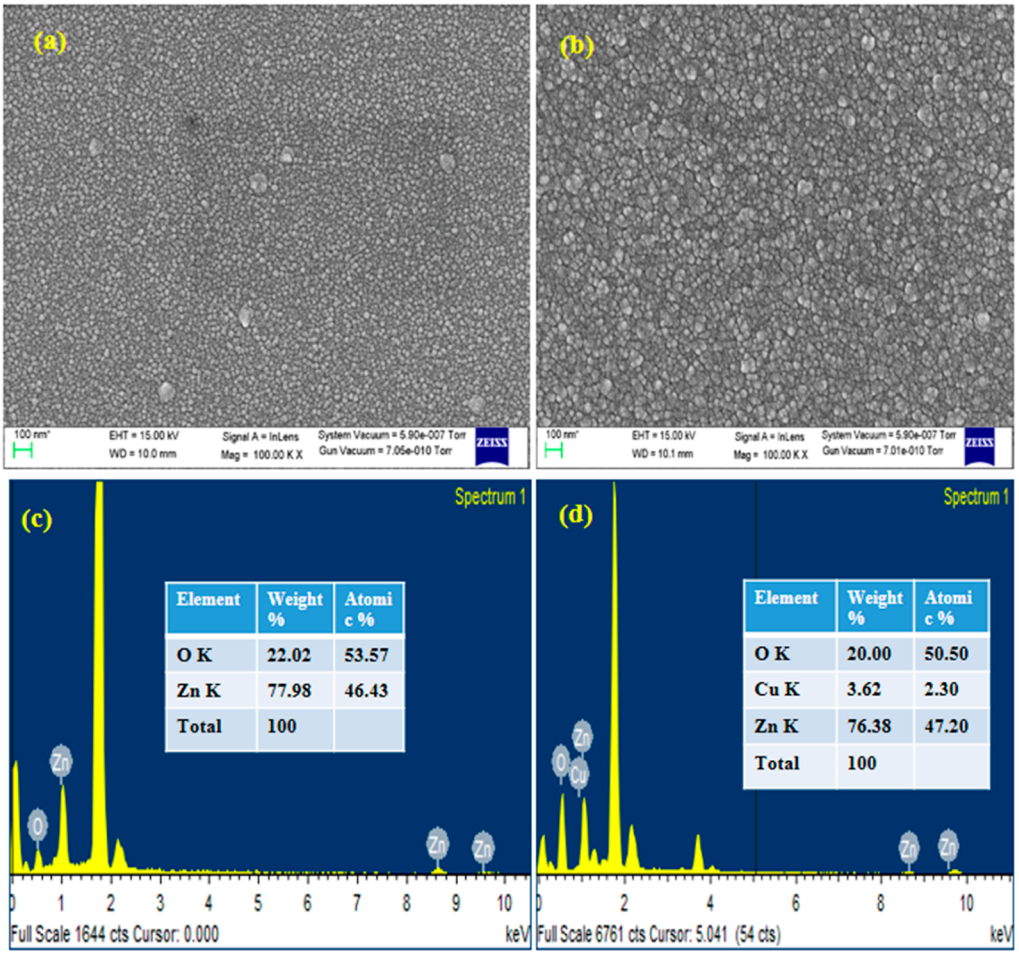

Figure 3. FESEM image of (a) UZO and (b) CZO thin films deposited on the Si substrate. EDX spectra of (c) UZO and (d) CZO thin films.

$$\varepsilon = \frac{\beta}{4\tan\theta} \tag{3}$$

For the UZO and CZO films, the microstrain values were found to be 4.05×10^{-3} and 5.07×10^{-3}, respectively.

Figure 3, displays field emission scanning electron microscopy (FESEM) images capturing the surface morphology of the thin films: (a) UZO and (b) CZO. In all instances, the results exhibit a finely crystalline arrangement on the nanometer scale, with grains densely packed together. It is observed that UZO films exhibited a porous structure of small grains in compare to CZO thin films. These distinctive granular patterns are consistently distributed across the film surfaces, devoid of any indications of cracks or pinholes. This collective observation provides compelling evidence for the successful fabrication of high quality CZO thin film nanostructures. Figure 3c,d presents the thin film EDX spectra, confirming the successful incorporation of copper in ZnO thin films. Surface roughness plays an important role in the photodetection performance of thin films. To evaluate the roughness, AFM analysis was performed. Figure 4a−d showcases the three- and two-dimensional AFM images of UZO and CZO thin films, scanned over a 5 μm × 5 μm surface area. It is evident from Figure 4a−d, that all samples exhibit uniform and dense ZnO grains, while the doping of copper increases the roughness of the ZnO thin films. The root-mean-square (RMS) roughness was found to be 1.4 nm for the UZO thin films and 4.2 nm for the CZO thin films. The photodetection performance of thin films can be influenced by surface roughness.[47] Therefore, the observed increase in roughness in CZO thin films compared with UZO thin films may have implications for their respective photodetection capabilities.

The optical properties of thin films are known to depend on their stoichiometry.[48] Figure 5a, displays the XPS core levels of UZO and CZO thin films, focusing on the Auger transitions and contaminated state (Zn 3s, Zn 3p, Zn 3d, C 1s, and Cu 2p). The analysis of these core levels provides insights into the elemental composition and oxidation states of the films. However, identifying Cu as a dopant in CZO thin films based solely on binding energy (BE) analysis is challenging as distinguishing between different oxidation states of Zn and Cu is not possible.[49,50] To determine the elemental chemical composition of UZO and CZO thin films, we calculated the composition using XPS signals of elements (C, O, Zn, and Cu). The highly symmetrical Zn 2p core level in Figure 5b, with binding energies of 1021.80 ± 0.10 eV for Zn $2p_{3/2}$ and 1043.80 ± 0.10 eV for Zn $2p_{1/2}$, confirms that the majority of Zn atoms in all films were in the Zn^{2+} valence state within the ZnO structure. The absence of a 1021.50 eV signal indicates the absence of metallic Zn, suggesting the presence of only the oxidized state of Zn. Figure 5c, shows asymmetric XPS spectra for UZO and CZO thin films corresponding to the O 1s core level, indicating the presence of multicomponent oxygen molecules. The deconvolution of these spectra into several subspectral components (Figure 5d,e) reveals different oxygen

https://doi.org/10.1021/acsomega.3c04091
ACS Omega 2023, 8, 36966−36977

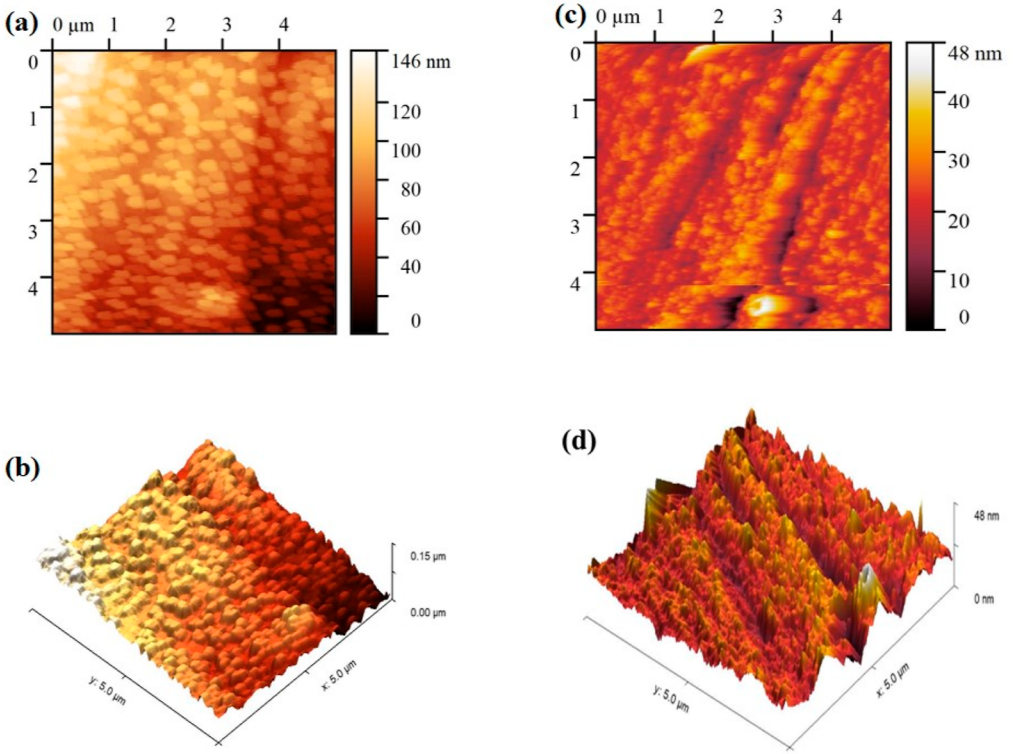

Figure 4. 2D and 3D AFM images of UZO thin films: (a, b) and CZO thin films: (c, d).

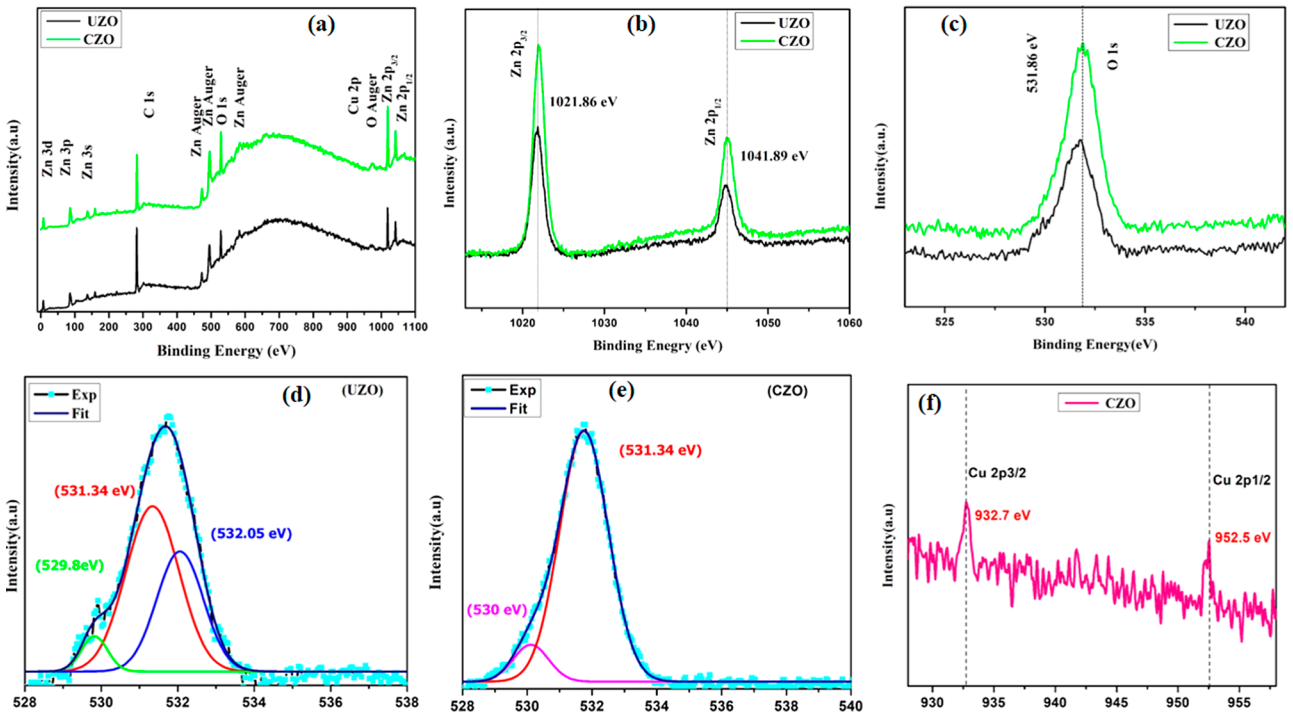

Figure 5. (a) XPS spectra of UZO and CZO thin films, (b) core-level XPS spectra of Zn 2p, (c) XPS spectra for UZO and CZO thin films corresponding to the O 1s core level, (d,e) deconvoluted XPS spectra of UZO and CZO thin films corresponding to the O 1s core level, and (f) Cu 2p XPS spectra of CZO thin films.

species, including O^{2-} ions in the wurtzite lattice with Zn^{2+} ions, oxygen-deficient regions with defective ZnO, ZnOH, and/or Cu−O−Zn, as well as loosely bound absorbed or interstitial oxygen in UZO thin films.[51,52]

In Figure 5f, the Cu 2p XPS spectra of the CZO thin film exhibit two prominent peaks: one at 932.7 eV corresponding to Cu $2p_{3/2}$ and another at 952.5 eV corresponding to Cu $2p_{1/2}$. According to literature sources, the peak at 952.5 eV is associated with metallic Cu and Cu^{+} cationic states, indicating

https://doi.org/10.1021/acsomega.3c04091
ACS Omega 2023, 8, 36966−36977

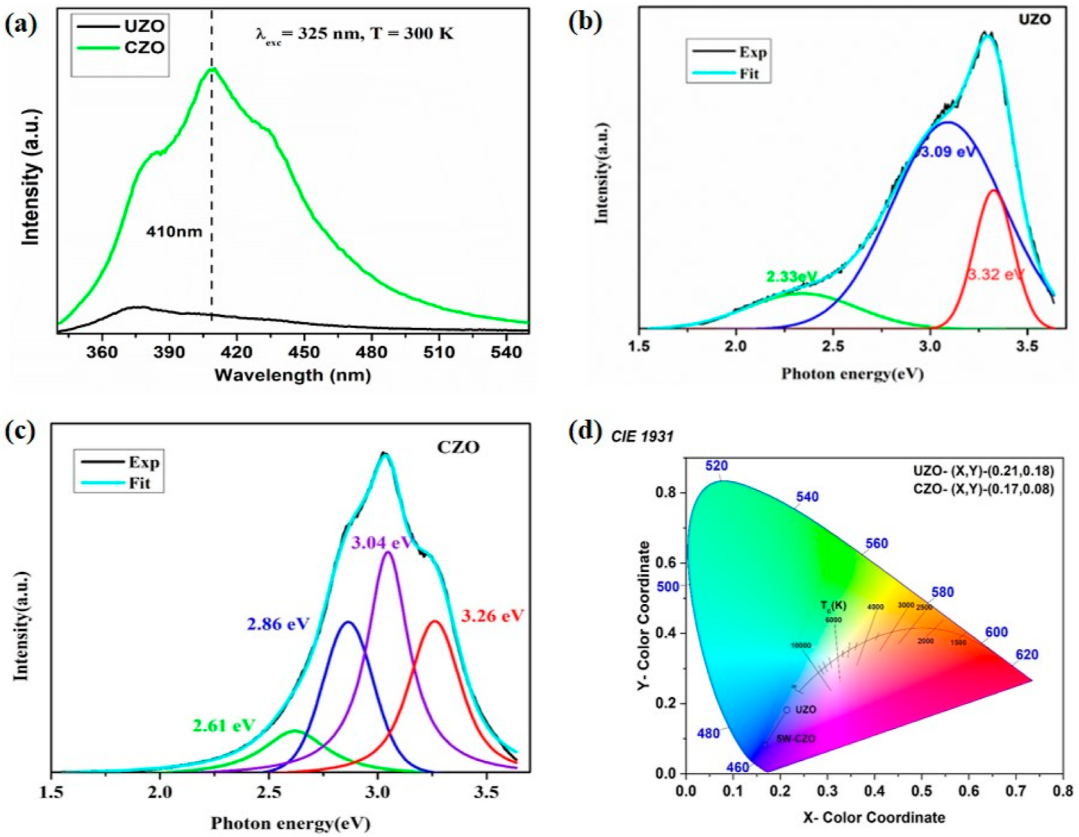

Figure 6. (a) RT-PL spectra of UZO and CZO thin films, (b,c) deconvoluted RT-PL spectra of UZO and CZO thin films, and (d) CIE chromaticity coordinates of UZO and CZO thin films.

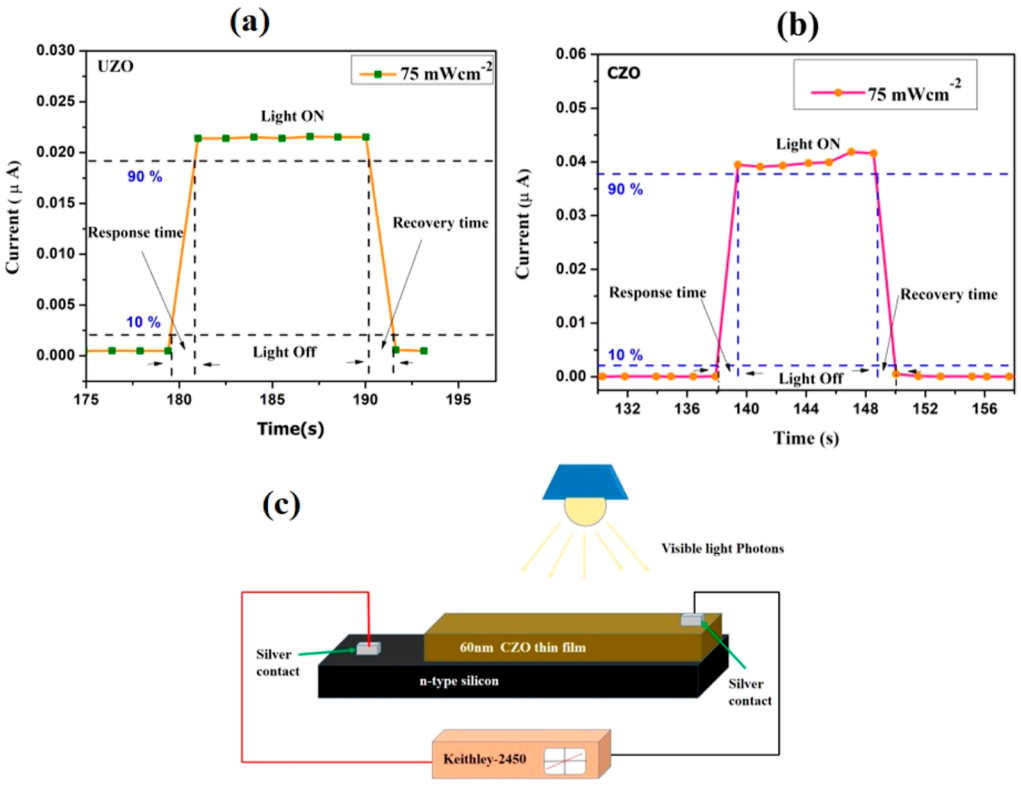

Figure 7. Response and recovery curves for a single cycle under 75 mW cm^{-2} visible light (on/off) of photodetector based on (a) UZO thin film and (b) CZO thin film. (c) Schematic diagram of the p-CZO/n-Si thin film-based.

https://doi.org/10.1021/acsomega.3c04091
ACS Omega 2023, 8, 36966−36977

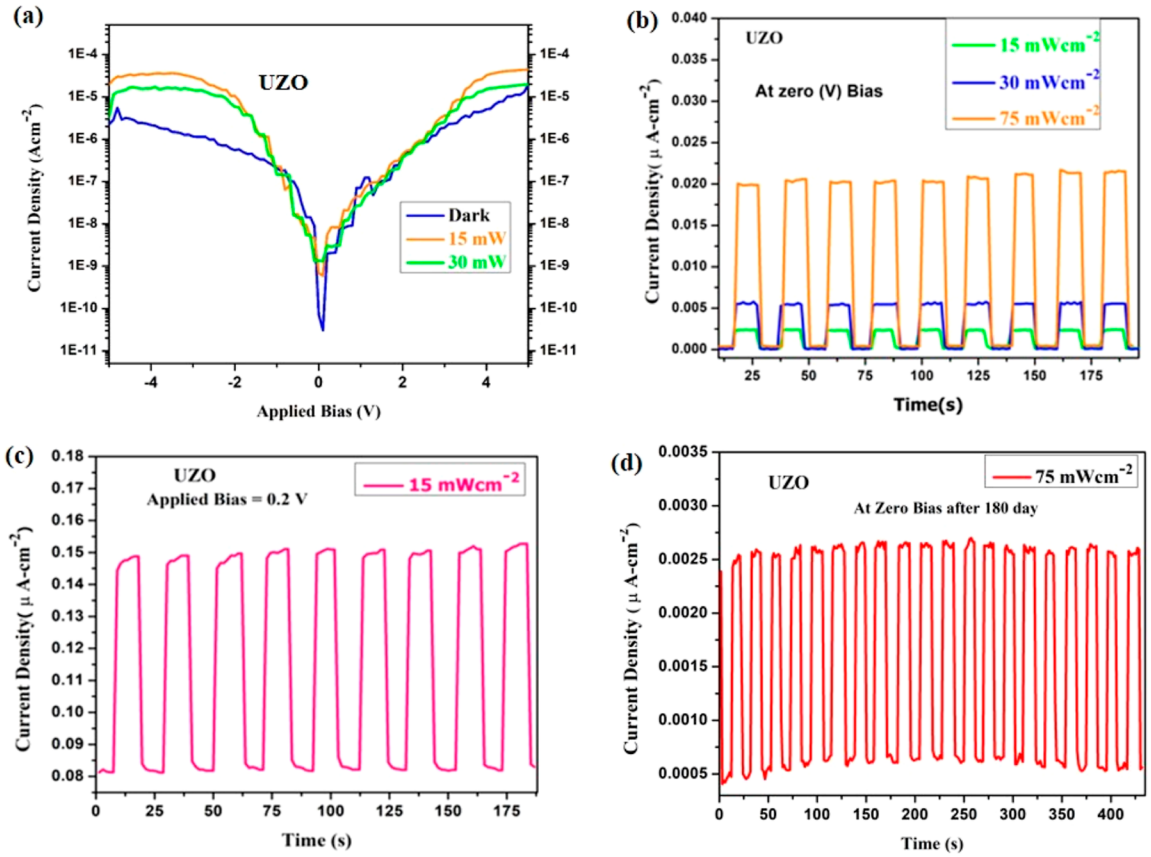

Figure 8. (a) $I-V$ characteristics curve at +5 to −5 V for the UZO/n-Si junction at room temperature, $I-t$ characteristics curve for the UZO sample in forward bias at (b) 0 V bias voltage with visible light (on/off) for 75, 30, and 15 mW, (c) 0.2 V bias voltage with visible light (on/off) for 15 mW, and (d) UZO sample photo response for 75 mW visible light after 180 days.

the presence of Cu in the samples in the forms of CuO or Cu−O−Zn. These XPS results further confirm the substitution of Zn^+ ions by Cu^+ ions in the CZO sample.[52,53] Moreover, the doping of Cu ions in CZO thin films enhances the photoconductivity compared with undoped films, contributing to improved photodetection performance.

For a detailed investigation of the defects induced in UZO and CZO thin films, photoluminescence (RT-PL) measurements at ambient temperature were done using a He−Cd laser at an excitation wavelength of 325 nm. Figure 6a illustrates the combined RT-PL spectra of UZO and CZO thin films for wavelengths of 340−650 nm. For UZO thin films, a strong UV emission peak centered at 376 nm (3.29 eV) has been observed, while in CZO thin films, broad visible (blue and violet) emission peaks have appeared at nearly 410 nm (3.02 eV). As the doping concentration has been increased, the intensity enhanced hastily. This increase in intensity may be because when the Cu^{2+} site is in the ZnO host lattice, Cu luminescence centers and native defects are created which raise the emission intensity.[54] A similar trend of results has been reported in previous research.[42,55] The peak centered at 376 nm is related to the near-band edge (NBE) free exciton transition.[56] The peak centered at nearly 410 nm, known as the DLE (deep-level-emission) peak, is due to various defects including the substitution of the Zn^{2+} ion and vacancies of oxygen and Zn interstitial.[57] For a more detailed investigation of these peaks, we deconvoluted RT-PL spectra of all samples, as shown in Figure 6b,c. It can be seen from Figure 6b that UZO thin film RT-PL spectra contain three luminescent centers that are at 3.32 eV (373 nm) UV emission, 3.09 eV (401 nm) violet emission, and 2.33 eV (532 nm) green emission, respectively, and for all CZO thin films, spectra contain four luminescent centers: one in UV emission (3.25 eV), two in blue emission (2.6 and 2.8 eV), and one in violet emission (3.04 eV), respectively. It is widely known that the excitonic NBE emission is responsible for the emission center's formation at around 3.32 eV (373 nm).[58] The violet emission band falling in the range of 3.04 eV is shown as the transition of electrons from the bottom of the conduction band (E_c) to the zinc vacancy (V_{Zn}) level.[59] The blue emission centered at 2.85 eV(435 nm) is caused by the transition of electrons from the conduction band to the Cu^+ acceptor level while the peak centered at 2.61 eV(475 nm) occurred due to the transition of electrons from the Cu^{2+} donor level to the Cu^+ acceptor level.[55] The green emission centered at 2.33 eV for the UZO sample is caused by oxygen vacancy defects.[57,60] Since in the CZO sample, no peak related to green emission has been found, we can thus say that doping of copper does not produce oxygen vacancy in CZO thin films; perhaps Cu substituted Zn in host ZnO, which is also confirmed by XRD and XPS results. A similar result was also reported by Singh et al.[61] and Sreedhar et al.[59] The color coordinates of PL on the CIE 1931 X−Y chromaticity diagram are shown in Figure 6d. The color points of the UZO and CZO thin films were found at (0.254, 0.0.175) and (0164, 0.026), correspondingly.

For photodetector application, UZO and CZO samples deposited on an n-type Si substrate with Ag electrodes are used and examined by a Keithley-2450 in the dark and visible light.

https://doi.org/10.1021/acsomega.3c04091
ACS Omega 2023, 8, 36966−36977

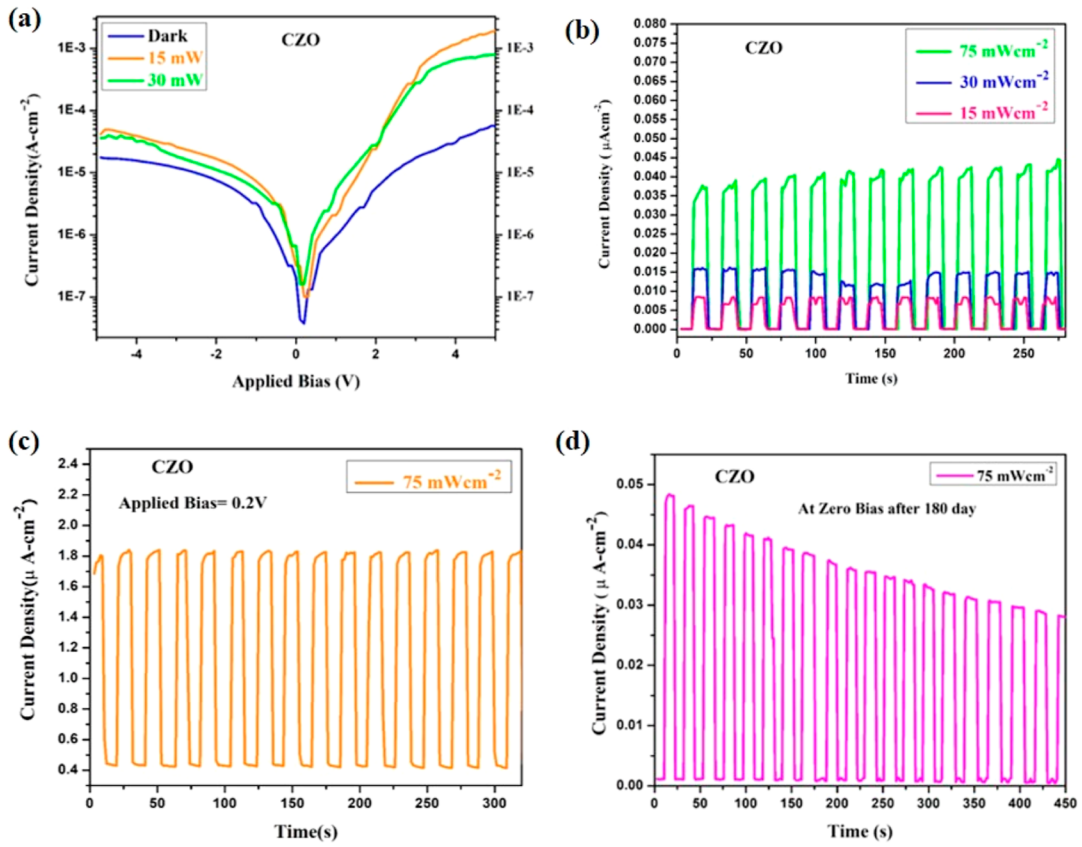

Figure 9. (a) $I-V$ characteristic curve at +5 V to −5 V for the CZO/n-Si junction at room temperature. $I-t$ characteristics curve for the CZO sample in forward bias at (b) zero bias voltage with visible light (on/off) for 75, 30, and 15 mW. (c) 0.2 V bias voltage with visible light (on/off) for 75 mW. (d) Photoresponse for 75 mW visible light after 180 days.

Table 2. Characteristic Parameters with Mathematical Formulas of PDs and the Photoresponse of CZO/n-Si and UZO/n-Si PDs with and without Bias at 75 mW Visible Light

		UZO		SW CZO		references (zero bias)	
parameter	mathematical relation unit	0 V bias	0.2 V bias	0 V bias	0.2 V bias	p-Si/n-ZnO[65]	Sn_3O_4[66]
response current A	$\Delta I = I_{light} - I_{dark}$	2.05×10^{-8}	6.7×10^{-8}	4.07×10^{-8}			
		40	0.8	1.37×10^{-8}		390	5×10^3
sensitivity unit less	$S = \frac{\Delta I}{I_{dark}}$			1.36×10^2	3		
response time s	$\tau_r = t_{90\%} - t_{10\%}$ (where $t_{10\%}$ and $t_{90\%}$ are the time at 10 and 90% of the saturation value)	1.30	1.31			34	0.35
				1.20	1.34		
		1.36	1.12	1.12	1.20	27	0.28
recovery time s	$\tau_d = t_{10\%} - t_{90\%}$	2.7×10^{-3}	2.9×10^{-3}	15×10^{-3}		1.83×10^{-3}	0.1×10^{-3}
				0.71			
responsivity A W^{-1}	$R_s = \frac{\Delta I}{PA}$	1.9×10^9				3.12×10^9	
		5.5×10^{10}					
				2.8×10^{10}			
				26×10^{10}			
specific detectivity Jones	$D = R_s \times \left(\frac{A_0}{2eI_{dark}}\right)^{1/2}$						

The Experimental Details section provides a detailed description of the fabrication process. All measurements were made in an air environment at ambient temperature. The schematic diagram of the photodetector setup is shown in Figure 7c. The $I-V$ characteristics of UZO/n-Si and CZO/n-Si thin films with and without light have been studied for −5 to +5 V and are shown in Figures 8a and 9a. The behavior of the log-scale $I-V$ graph for UZO/n-Si thin film has been found to be nearly symmetric, which represents a conventional metal−semiconductor−metal (MSM) behavior of photodetectors. On

https://doi.org/10.1021/acsomega.3c04091
ACS Omega 2023, 8, 36966−36977

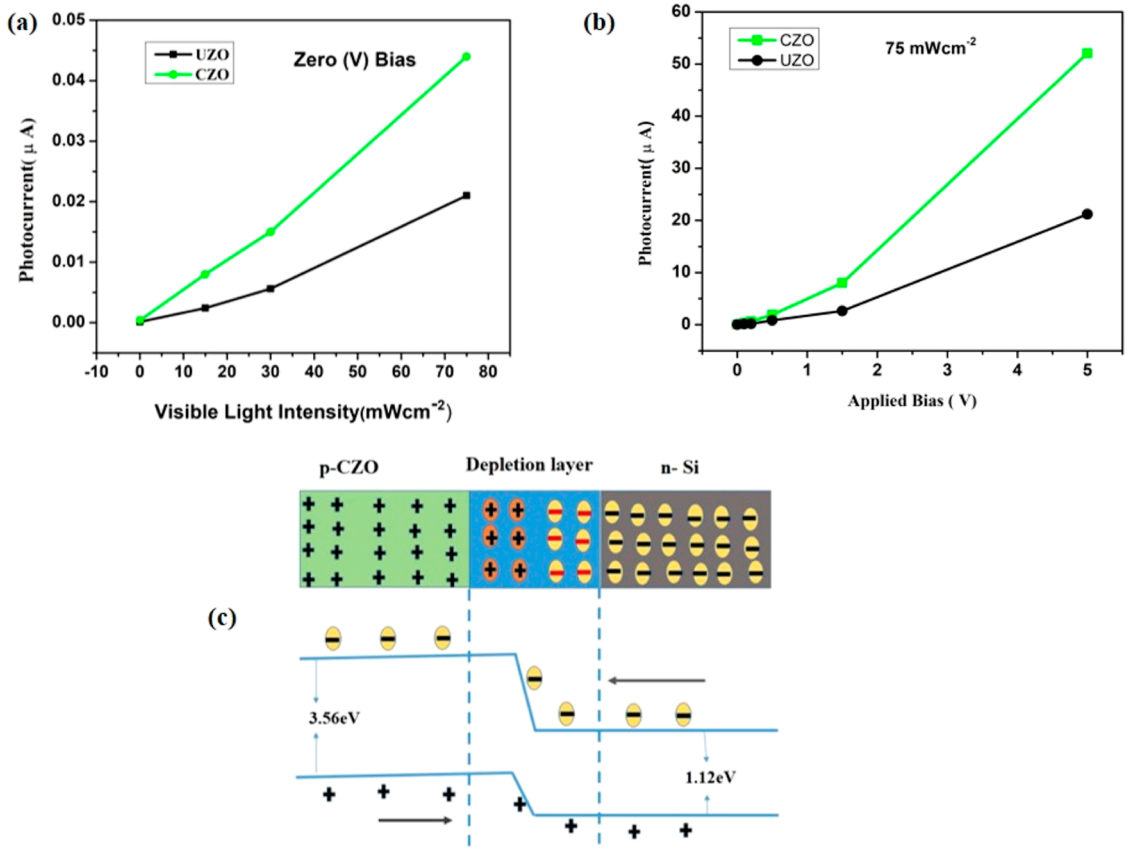

Figure 10. (a) Incident visible light intensity vs photocurrent for UZO and CZO thin films at zero applied bias, (b) applied bias vs photocurrent at 75 mW cm^{-2} visible-light intensity, and (c) energy band diagram of the CZO/n-Si heterojunction photodetector under visible-light illumination at zero bias voltage.

the other hand, the log-scale $I-V$ graph of CZO/n-Si shows a nonsymmetric behavior, which suggests that a rectified p−n junction formed between the CZO thin film and the n-Si layer. The literature says that conventional MSM-based PDs show a higher dark current, slow response and recovery, and a higher recombination rate of photo charge carriers with visible light,[62,63] while a Schottky barrier-based PD has a comparatively low dark current, quick response and recovery time, and a controlled photoresponse performance.[64]

The performance of both PDs was calculated by important parameters like response time, recovery time, response current, sensitivity, responsivity, and specific detectivity, as summarized in Table 2. Table 2 also briefly compares our results with some previous works' results. It is clearly shown in Table 2 that the doping of copper enhances all the photoconduction parameters; i.e., CZO/n-Si shows better photoconduction than UZO/n-Si. Figure 9b shows $I-t$ curves of the 5W CZO/n-Si sample at zero bias voltage for 75, 30, and 15 mW cm^{-2} visible light illumination (On/Off). The photocurrent rises very fast from 8 to 37 nA as the intensity of the incident increases from 15 to 75 mW cm^{-2}. On the other hand, for UZO/n-Si, the rise in photocurrent is comparatively slow; it rises from 2.3 to 18 nA as the incident light intensity increases from 15 to 75 mW cm^{-2}, as shown in Figure 8b. Figures 8c and 9c are $I-t$ curves with 0.2 V forward bias voltage at 75 mW cm^{-2} visible light (On/Off) for CZO/n-Si and UZO/n-Si, respectively. The energy band structure of the heterojunction is depicted in Figure 10c to explain the operation of the self-operating CZO/n-Si photodetector. The electron−hole pairs may form in response to visible light, and when they are swiftly separated by the built-in field in the depletion area, the dynamic equilibrium is disrupted, resulting in the generation of a photoinduced voltage. Stable photocurrent will result from the transfer of holes from n-Si to the valence band of the CZO layer and the movement of electrons from the conduction band of CZO to the Ag electrode. The Ag electrodes may collect the carriers independently, generating a current loop that is driven by the photoinduced voltage, allowing the device to function as a self-operating photodetector.[41]

Also, PD-specific detectivity has an important role for CZO/n-Si detectivity enhances 6.7% more than UZO/n-Si. The responsivity of CZO/n-Si also increases by 18% compared to that of UZO/n-Si. Now, the literature says that the stability of a PD is a challenge. For stability testing, we take 20 cycles of the $I-t$ curve at zero bias after 180 days, as shown in Figures 8c and 9c. It is clear from Figure 9c that CZO/n-Si behaves the same after 180 days as it did before; a photocurrent at 75 mW cm^{-2} with zero bias has found 36 nA, which is almost the same as that before 180 days (37 nm). The on/off ratio change after 180 is less than 5%.

Figure 10a presents the variation in the photocurrent with the intensity of incident visible light at zero bias for UZO/n-Si and CZO/n-Si photodetectors. The CZO/n-Si photodetector exhibits a faster rise in photocurrent compared to UZO/n-Si. Figure 10b depicts the behavior of the photocurrent as the applied bias is varied at 75 mW cm^{-2}. Both the UZO/n-Si and CZO/n-Si photodetectors show an approximately linear increase in photocurrent as the applied bias increases from 0

https://doi.org/10.1021/acsomega.3c04091
ACS Omega 2023, 8, 36966−36977

to 5 V. However, the rise in photocurrent is more pronounced for CZO/n-Si compared to UZO/n-Si. Therefore, the CZO/n-Si-based photodetector demonstrates high reproducibility and stability, with a rapid response and decay time in the self-operating mode for over 180 days. The response/recovery time, specific detectivity, and responsivity of the CZO/n-Si photodetector are comparable to or even enhanced compared to the works of Karthick et al.,[65] Xia et al.,[66] and Elkamel et al.[67]

4. CONCLUSIONS

This study includes a comparative analysis of self-powered photodetectors based on CZO and UZO thin films grown on a silicon substrate. The synthesis of uniform, highly adhesive, and transparent CZO and UZO thin films was achieved at room temperature using reactive cosputtering of pure Zn and Cu targets. The structural characterization revealed a hexagonal wurtzite structure, primarily on the (002) plane, for all of the thin films. EDS and XPS analyses confirmed the successful doping of Cu in the CZO samples. The presence of defects was evaluated through room-temperature photoluminescence spectra. Upon comparing CZO/n-Si- and UZO/n-Si-based photodetectors, the CZO/n-Si configuration exhibited superior performance, featuring a high on/off ratio of approximately 300 and a specific detectivity of 2.8×10^{10} Jones under a visible light intensity of 75 mW cm^{-2}. Additionally, the CZO/n-Si photodetector demonstrated excellent reproducibility and stability, maintaining its response and recovery time in the self-powered mode for more than 180 days. Moreover, at a bias of 0.2 V, the CZO/n-Si photodetector displayed a high responsivity of 0.71 A W^{-1}. CZO/n-Si-based photodetectors exhibited improved photoconductivity compared to their UZO/n-Si counterparts. The successful fabrication and superior performance of CZO/n-Si photodetectors open new avenues for cost-effective and high-performance self-powered photodetection.

AUTHOR INFORMATION

Corresponding Authors

Beer Pal Singh − *Department of Physics, Chaudhary Charan Singh University, Meerut 250004, India;* orcid.org/0000-0002-1646-8404; Email: drbeerpal@gmail.com

Ashwani Kumar − *Nanoscience Laboratory, Institute Instrumentation Centre, IIT Roorkee, Roorkee 247667, India; Department of Physics, Graphic Era Deemed to be University, Dehradun, Uttarakhand 248002, India;* orcid.org/0000-0003-3798-6486; Email: 01ashraj@gmail.com

Authors

Manohar Singh − *Department of Physics, Chaudhary Charan Singh University, Meerut 250004, India*

Anit Kumar Ambedkar − *Department of Physics, Chaudhary Charan Singh University, Meerut 250004, India*

Shrestha Tyagi − *Department of Physics, Chaudhary Charan Singh University, Meerut 250004, India*

Arun Kumar − *Department of Applied Physics, Amity Institute of Applied Science(AIAS), Amity University, Noida, Uttar Pradesh 201303, India*

Yogendra K. Gautam − *Department of Physics, Chaudhary Charan Singh University, Meerut 250004, India;* orcid.org/0000-0003-4662-4583

Kavita Sharma − *Department of Physics, Chaudhary Charan Singh University, Meerut 250004, India*

Complete contact information is available at: https://pubs.acs.org/10.1021/acsomega.3c04091

Notes

The authors declare no competing financial interest.

ACKNOWLEDGMENTS

The authors would also like to acknowledge UGC and CSIR New Delhi, India, for financial assistance [file no.: 16-9 (June 2017)/2018(NET/CSIR)]. Dr. Ashwani Kumar expresses sincere appreciation to CSIR-SRA (Pool Scientist), New Delhi, for their generous funding [grant no. 13(9131)-A/2020-Pool], which provided the necessary financial assistance to conduct this research.

REFERENCES

(1) Thongma, S.; Tantisantisom, K.; Grisdanurak, N.; Boonkoom, T. UV Enhanced White-Light Response Based on p-Si/n-ZnO Nanorod Heterojunction Photosensor. *Sens. Actuators, A* **2019**, *296*, 324−330.

(2) Zheng, W.; Bian, T.; Li, X.; Chen, M.; Yan, X.; Dai, Y.; He, G. A Self-Powered Ultraviolet Photodetector Driven by Opposite Schottky Junction. *J. Alloys Compd.* **2017**, *712*, 425−430.

(3) Khokhra, R.; Bharti, B.; Lee, H. N.; Kumar, R. Visible and UV Photo-Detection in ZnO Nanostructured Thin Films via Simple Tuning of Solution Method. *Sci. Rep.* **2017**, *7* (1), 15032−15114.

(4) Patel, M.; Kim, J. Transparent NiO/ZnO Heterojunction for Ultra-Performing Zero-Bias Ultraviolet Photodetector on Plastic Substrate. *J. Alloys Compd.* **2017**, *729*, 796−801.

(5) Hao, L.; Xu, H.; Dong, S.; Du, Y.; Luo, L.; Zhang, C.; Liu, H.; Wu, Y.; Liu, Y. SnSe/SiO2/Si Heterostructures for Ultrahigh-Sensitivity and Broadband Optical Position Sensitive Detectors. *IEEE Electron Device Lett.* **2019**, *40* (1), 55−58.

(6) Chen, X.; Liu, K.; Zhang, Z.; Wang, C.; Li, B.; Zhao, H.; Zhao, D.; Shen, D. Self-Powered Solar-Blind Photodetector with Fast Response Based on Au/β-Ga2O3 Nanowires Array Film Schottky Junction. *ACS Appl. Mater. Interfaces* **2016**, *8* (6), 4185−4191.

(7) Garnier, J.; Parize, R.; Appert, E.; Chaix-Pluchery, O.; Kaminski-Cachopo, A.; Consonni, V. Physical Properties of Annealed ZnO Nanowire/CuSCN Heterojunctions for Self-Powered UV Photodetectors. *ACS Appl. Mater. Interfaces* **2015**, *7* (10), 5820−5829.

(8) Sheng, X.; Yu, C.; Malyarchuk, V.; Lee, Y. H.; Kim, S.; Kim, T.; Shen, L.; Horng, C.; Lutz, J.; Giebink, N. C.; Park, J.; Rogers, J. A. Silicon-Based Visible-Blind Ultraviolet Detection and Imaging Using down-Shifting Luminophores. *Adv. Opt. Mater.* **2014**, *2* (4), 314−319.

(9) Aggarwal, N.; Krishna, S.; Sharma, A.; Goswami, L.; Kumar, D.; Husale, S.; Gupta, G. A Highly Responsive Self-Driven UV Photodetector Using GaN Nanoflowers. *Adv. Electron. Mater.* **2017**, *3* (5), 1−7.

(10) Shakya, P.; Saxena, A.; Saxena, P. K.; Gupta, F. K.; Srivastava, A.; Srivastava, P.; Dixit, M.; Gambhir, S.; Shukla, R. K.; Srivastava, A. An Innovative Technique for Electronic Transport Model of Group - III Nitrides. *Sci. Rep.* **2020**, *10*, 18706−18712.

(11) Zhan, Z.; Zheng, L.; Pan, Y.; Sun, G.; Li, L. Self-Powered, Visible-Light Photodetector Based on Thermally Reduced Graphene Oxide-ZnO (RGO-ZnO) Hybrid Nanostructure. *J. Mater. Chem.* **2012**, *22* (6), 2589−2595.

(12) Konstantatos, G.; Sargent, E. H. Nanostructured Materials for Photon Detection. *Nat. Nanotechnol.* **2010**, *5* (6), 391−400.

(13) Ahamad, T.; Majeed Khan, M. A.; Kumar, S.; Ahamed, M.; Shahabuddin, M.; Alhazaa, A. N. CdS Quantum Dots: Growth, Microstructural, Optical and Electrical Characteristics. *Appl. Phys. B: Laser Opt.* **2016**, *122*, 179.

(14) Zheng, M.; Gui, P.; Wang, X.; Zhang, G.; Wan, J.; Zhang, H.; Fang, G.; Wu, H.; Lin, Q.; Liu, C. ZnO Ultraviolet Photodetectors

with an Extremely High Detectivity and Short Response Time. *Appl. Surf. Sci.* **2019**, *481*, 437−442.
(15) Zhang, Z.; Liao, Q.; Yu, Y.; Wang, X.; Zhang, Y. Enhanced Photoresponse of ZnO Nanorods-Based Self-Powered Photodetector by Piezotronic Interface Engineering. *Nano Energy* **2014**, *9*, 237−244.
(16) Huang, J.; Jiang, J.; Hu, L.; Zeng, Y.; Ruan, S.; Ye, Z.; Zeng, Y. J. Self-Powered Ultraviolet Photodetector Based on CuGaO/ZnSO Heterojunction. *J. Mater. Sci.* **2020**, *55* (21), 9003−9013.
(17) Hu, L.; Liao, Q.; Xu, Z.; Yuan, J.; Ke, Y.; Zhang, Y.; Zhang, W.; Wang, G. P.; Ruan, S.; Zeng, Y. J.; Han, S. T. Defect Reconstruction Triggered Full-Color Photodetection in Single Nanowire Phototransistor. *ACS Photonics* **2019**, *6* (4), 886−894.
(18) Katiyar, A.; Kumar, N.; Shukla, R. K.; Srivastava, A. Synergistic Effect of Fe and Ag Co-Doping on the Persistent Photoconductivity of Vertical ZnO Nanorods. *Ceram. Int.* **2022**, *48* (16), 23002−23015.
(19) Katiyar, A.; Kumar, N.; Shukla, R. K.; Srivastava, A. Growth and Study of C-Axis-Oriented Vertically Aligned ZnO Nanorods on Seeded Substrate. *J. Mater. Sci. Mater. Electron.* **2021**, *32* (12), 15687−15706.
(20) Katiyar, A.; Kumar, N.; Shukla, R. K.; Srivastava, A. Substrate Free Ultrasonic-Assisted Hydrothermal Growth of ZnO Nanoflowers at Low Temperature. *SN Appl. Sci.* **2020**, *2* (8), 1386.
(21) Kumar, V.; Prakash, J.; Pathak, D.; Sharma, D. P.; Purohit, L. P.; Swart, H. C. Ion Beam Engineering of Implanted ZnO Thin Films for Solar Cell and Lighting Applications. *Chem. Eng. J. Adv.* **2023**, *15*, 100501.
(22) Kumar, N.; Katiyar, A.; Shukla, R. K. A. S.; Srivastava, A. Enhancement in Visible Emission by the Doping of Ce in ZnO Thin Films. *J. Nano- Electron. Phys.* **2021**, *13*, 02011-1−02011-3.
(23) Katiyar, A.; Kumar, N.; Shukla, R.; Srivastava, A. Materials Today: Proceedings Substrate Free Defect-Rich One Dimensional ZnO Nanostructures. *Mater. Today Proc.* **2021**, *46*, 2374−2378.
(24) Saxena, P. K.; Srivastava, A.; Saxena, A.; Gupta, F.; Shakya, P.; Srivastava, A.; Shukla, R. K. An Innovative Model for Electronic Band Structure Analysis of Doped and Un-Doped ZnO. *J. Electron. Mater.* **2021**, *50* (4), 2417−2424.
(25) Choudhary, K.; Saini, R.; Upadhyay, G. K.; Rana, V. S.; Purohit, L. P. Wrinkle Type Nanostructured Y-Doped ZnO Thin Films for Oxygen Gas Sensing at Lower Operating Temperature. *Mater. Res. Bull.* **2021**, *141*, 111342.
(26) Pathak, T. K.; Kumar, V.; Swart, H.; Purohit, L. Electrical and Optical Properties of P-Type Codoped ZnO Thin Films Prepared by Spin Coating Technique. *Phys. E* **2016**, *77*, 1−6.
(27) Doni Pon, V.; Joseph Wilson, K. S.; Hariprasad, K.; Ganesh, V.; Elhosiny Ali, H.; Algarni, H.; Yahia, I. S. Enhancement of Optoelectronic Properties of ZnO Thin Films by Al Doping for Photodetector Applications. *Superlattice. Microst.* **2021**, *151*, 106790.
(28) Padmavathy, V.; Sankar, S. Tuning the Optical Properties of ZnO:Cd by Doping La and Y. *Superlattice. Microst.* **2019**, *128*, 127−135.
(29) Owoeye, V. A.; Ajenifuja, E.; Adeoye, E. A.; Osinkolu, G. A.; Popoola, A. P. Microstructural and Optical Properties of Ni-Doped ZnO Thin Films Prepared by Chemical Spray Pyrolysis Technique. *Mater. Res. Express* **2019**, *6* (8), 086455.
(30) Bairy, R.; Patil, P. S.; Maidur, S. R.; Vijeth, H.; Murari, M. S.; Bhat K, U. The Role of Cobalt Doping in Tuning the Band Gap, Surface Morphology and Third-Order Optical Nonlinearities of ZnO Nanostructures for NLO Device Applications. *RSC Adv.* **2019**, *9* (39), 22302−22312.
(31) López-Suárez, A.; Acosta, D.; Magaña, C.; Hernández, F. Optical, Structural and Electrical Properties of ZnO Thin Films Doped with Mn. *J. Mater. Sci. Mater. Electron.* **2020**, *31* (10), 7389−7397.
(32) Rana, V. S.; Rajput, J. K.; Pathak, T. K.; Purohit, L. P. Multilayer MgZnO/ZnO Thin Films for UV Photodetectors. *J. Alloys Compd.* **2018**, *764*, 724−729.
(33) Ong, W. L.; Huang, H.; Xiao, J.; Zeng, K.; Ho, G. W. Tuning of Multifunctional Cu-Doped ZnO Films and Nanowires for Enhanced Piezo/Ferroelectric-like and Gas/Photoresponse Properties. *Nanoscale* **2014**, *6* (3), 1680−1690.
(34) Xu, C. X.; Sun, X. W.; Zhang, X. H.; Ke, L.; Chua, S. J. Photoluminescent Properties of Copper-Doped Zinc Oxide Nanowires. *Nanotechnology* **2004**, *15* (7), 856−861.
(35) Suja, M.; Bashar, S. B.; Morshed, M. M.; Liu, J. Realization of Cu-Doped p-Type ZnO Thin Films by Molecular Beam Epitaxy. *ACS Appl. Mater. Interfaces* **2015**, *7* (16), 8894−8899.
(36) Rahmani, M. B.; Keshmiri, S. H.; Shafiei, M.; Latham, K.; Wlodarski, W.; du Plessis, J.; Kalantar-Zadeh, K. Transition from N- to p-Type of Spray Pyrolysis Deposited Cu Doped ZnO Thin Films for NO2 Sensing. *Sens. Lett.* **2009**, *7* (4), 621−628.
(37) Kumar, N.; Kumar, R.; Kumar, S.; Chakarvarti, S. K. Structural and Electrical Studies of Template Synthesized Copper Nanowires. *Curr. Appl. Phys.* **2014**, *14* (11), 1547−1552.
(38) Wang, X. B.; Song, C.; Geng, K. W.; Zeng, F.; Pan, F. Photoluminescence and Raman Scattering of Cu-Doped ZnO Films Prepared by Magnetron Sputtering. *Appl. Surf. Sci.* **2007**, *253* (16), 6905−6909.
(39) Hu, L.; Zhu, L.; He, H.; Guo, Y.; Pan, G.; Jiang, J.; Jin, Y.; Sun, L.; Ye, Z. Colloidal Chemically Fabricated ZnO: Cu-Based Photodetector with Extended UV-Visible Detection Waveband. *Nanoscale* **2013**, *5* (20), 9577−9581.
(40) Hsu, C. L.; Gao, Y. D.; Chen, Y. S.; Hsueh, T. J. Vertical P-Type Cu-Doped ZnO/n-Type ZnO Homojunction Nanowire-Based Ultraviolet Photodetector by the Furnace System with Hotwire Assistance. *ACS Appl. Mater. Interfaces* **2014**, *6* (6), 4277−4285.
(41) Saini, M.; Singh, R.; Mitra, A.; Som, T. Photoresponse of Pulsed Laser Deposited ZnO:Cu Thin Films. *Sol. Energy* **2020**, *207* (June), 228−234.
(42) Drmosh, Q. A.; Rao, S. G.; Yamani, Z. H.; Gondal, M. A. Crystalline Nanostructured Cu Doped ZnO Thin Films Grown at Room Temperature by Pulsed Laser Deposition Technique and Their Characterization. *Appl. Surf. Sci.* **2013**, *270*, 104−108.
(43) Singh, M.; Ambedkar, A. K.; Tyagi, S.; Kumar, V.; Yadav, P.; Kumar, A.; Gautam, Y. K.; Singh, B. P. Room Temperature Photoluminescence and Spectroscopic Ellipsometry of Reactive Co-Sputtered Cu-Doped ZnO Thin Films. *Optik* **2022**, *257*, 168860.
(44) Kouklin, N. Cu-Doped ZnO Nanowires for Efficient and Multispectral Photodetection Applications. *Adv. Mater.* **2008**, *20* (11), 2190−2194.
(45) Ambedkar, A. K.; Singh, M.; Kumar, V.; Kumar, V.; Singh, B. P.; Kumar, A.; Gautam, Y. K. Structural, Optical and Thermoelectric Properties of Al-Doped ZnO Thin Films Prepared by Spray Pyrolysis. *Surface. Interfac.* **2020**, *19*, 100504.
(46) Tyagi, S.; Kumar, A.; Singh, M.; Sanger, A.; Singh, B. P. Defects Induced Photoluminescence and Ellipsometric Measurements of Reactive Sputtered Growth MoS_2 Nanoworms. *Opt. Mater.* **2021**, *113*, 110848.
(47) Tadeo, I. J. Materials Advances Films Synthesized by DC Reactive Sputtering on Different Substrates. *Adv. Mater.* **2021**, *2*, 3726−3735.
(48) Jaiswal, J.; Mourya, S.; Malik, G.; Chandra, R. Ellipsometric Investigation of Room Temperature Grown Highly-Oriented Anatase TiO2 Thin Films. *J. Electron. Mater.* **2019**, *48* (2), 1223−1234.
(49) Biesinger, M. C.; Lau, L. W. M.; Gerson, A. R.; Smart, R. S. C. Resolving Surface Chemical States in XPS Analysis of First Row Transition Metals, Oxides and Hydroxides: Sc, Ti, V, Cu and Zn. *Appl. Surf. Sci.* **2010**, *257* (3), 887−898.
(50) Briggs, D. X-Ray Photoelectron Spectroscopy (XPS). *Handbook of Adhesion*, 2nd ed, 2005; pp 621−622.
(51) Younas, M.; Shen, J.; He, M.; Lortz, R.; Azad, F.; Akhtar, M. J.; Maqsood, A.; Ling, F. C. C. Role of multivalent Cu, oxygen vacancies and CuO nanophase in the ferromagnetic properties of ZnO:Cu thin films. *RSC Adv.* **2015**, *5*, 55648−55657.
(52) Chow, L.; Lupan, O.; Chai, G.; Khallaf, H.; Ono, L. K.; Roldan Cuenya, B.; Tiginyanu, I. M.; Ursaki, V.; Sontea, V.; Schulte, A. Sensors and Actuators A: Physical Synthesis and Characterization of Cu-Doped ZnO One-Dimensional Structures for Miniaturized Sensor

https://doi.org/10.1021/acsomega.3c04091
ACS Omega 2023, 8, 36966−36977

Applications with Faster Response. *Sens. Actuators, A* **2013**, *189*, 399−408.
(53) Tahir, D.; Hasanuddin, U. Electronic and Optical Properties of Cu, CuO and Cu2O Studied by Electron Spectroscopy. *J. Phys.: Condens. Matter* **2017**, *24*, 175002.
(54) Raji, R.; Gopchandran, K. G. ZnO:Cu Nanorods with Visible Luminescence: Copper Induced Defect Levels and Its Luminescence Dynamics. *Mater. Res. Express* **2017**, *4* (2), 025002.
(55) Xu, L.; Xian, F.; Zheng, G.; Lai, M. Realization of Strong Violet and Blue Emissions from ZnO Thin Films by Incorporation of Cu Ions. *Mater. Res. Bull.* **2018**, *99*, 144−151.
(56) Licurgo, J. S. C.; Almeida Neto, G. R. d.; Paes Junior, H. R. Structural, Electrical and Optical Properties of Copper-Doped Zinc Oxide Films Deposited by Spray Pyrolysis. *Ceramica* **2020**, *66* (379), 284−290.
(57) Dejam, L.; Kulesza, S.; Sabbaghzadeh, J.; Ghaderi, A.; Solaymani, S.; Ţălu, Ş.; Bramowicz, M.; Amouamouha, M.; shayegan, A. h. S.; Sari, A. h. ZnO, Cu-Doped ZnO, Al-Doped ZnO and Cu-Al Doped ZnO Thin Films: Advanced Micro-Morphology, Crystalline Structures and Optical Properties. *Results Phys.* **2023**, *44*, 106209.
(58) Naouar, M.; Ka, I.; Gaidi, M.; Alawadhi, H.; Bessais, B.; Khakani, M. Growth, Structural and Optoelectronic Properties Tuning of Nitrogen-Doped ZnO Thin Films Synthesized by Means of Reactive Pulsed Laser Deposition. *Mater. Res. Bull.* **2014**, *57*, 47−51.
(59) Sreedhar, A.; Kwon, J. H.; Yi, J.; Kim, J. S.; Gwag, J. S. Enhanced Photoluminescence Properties of Cu-Doped ZnO Thin Films Deposited by Simultaneous RF and DC Magnetron Sputtering. *Mater. Sci. Semicond. Process.* **2016**, *49*, 8−14.
(60) Agarwal, D. C.; Singh, U. B.; Gupta, S.; Singhal, R.; Kulriya, P. K.; Singh, F.; Tripathi, A.; Singh, J.; Joshi, U. S.; Avasthi, D. K. Enhanced Room Temperature Ferromagnetism and Green Photoluminescence in Cu Doped ZnO Thin Film Synthesised by Neutral Beam Sputtering. *Sci. Rep.* **2019**, *9* (1), 6675−6712.
(61) Singh, M.; Ambedkar, A. K.; Tyagi, S.; Kumar, V.; Yadav, P.; Kumar, A.; Gautam, Y. K.; Singh, B. P. Room Temperature Photoluminescence and Spectroscopic Ellipsometry of Reactive Co-Sputtered Cu-Doped ZnO Thin Films. *Optik* **2022**, *257*, 168860.
(62) Deka Boruah, B. Zinc Oxide Ultraviolet Photodetectors: Rapid Progress from Conventional to Self-Powered Photodetectors. *Nanoscale Adv.* **2019**, *1* (6), 2059−2085.
(63) Kumar, A.; Mukherjee, S.; Sharma, H.; Rana, D. K.; Kumar, A.; Kumar, R.; Choubey, R. K. Fabrication of Low-Cost and Fast-Response Visible Photodetector Based on ZnS:Mn/p-Si Heterojunction. *Mater. Sci. Semicond. Process.* **2023**, *155*, 107226.
(64) Guo, D. Y.; Wu, Z. P.; An, Y. H.; Guo, X. C.; Chu, X. L.; Sun, C. L.; Li, L. H.; Li, P. G.; Tang, W. H. Oxygen Vacancy Tuned Ohmic-Schottky Conversion for Enhanced Performance in - Ga2O3 Solar-Blind Ultraviolet Photodetectors. *Appl. Phys. Lett.* **2014**, *105* (2), 023507.
(65) Karthick, K.; Kathirvel, P.; Marnadu, R.; Chakravarty, S.; Shkir, M. Ultrafast One Step Direct Injection Flame Synthesis of Zinc Oxide Nanoparticles and Fabrication of P-Si/n-ZnO Photodiode and Characterization. *Phys. B* **2021**, *612*, 412971.
(66) Xia, W.; Qian, H.; Zeng, X.; Dong, J.; Wang, J.; Xu, Q. Visible-Light Self-Powered Photodetector and Recoverable Photocatalyst Fabricated from Vertically Aligned Sn3O4 Nanoflakes on Carbon Paper. *J. Phys. Chem. C* **2017**, *121* (35), 19036−19043.
(67) Elkamel, I. B.; Hamdaoui, N.; Mezni, A.; Ajjel, R.; Beji, L. Effects of Plasmon Resonance on the Low Frequency Noise and Optoelectronic Properties of Au/Cu Codoped ZnO Based Photodetectors. *Opt. Quant. Electron.* **2023**, *55* (2), 148.

https://doi.org/10.1021/acsomega.3c04091
ACS Omega 2023, 8, 36966−36977